 doi:10.20944/preprints202210.0293.v1

Communication

Air Acoustic Sensing based on High-performance DAS and Ultra-simple Transducer Structure

Jianfang Tang [1], Minghao Hu [2], Xuanyu Zheng [2] and Fei Peng [2,*]

[1] CGN New Energy Holding Co. Ltd, Beijing, China; tjf_cgn@126.com
[2] College of Electrical Engineering, Sichuan University, Chengdu, China; pengfei@scu.edu.cn
* Correspondence: pengfei@scu.edu.cn

Featured Application: This work can be applied to the industrial field where DAS has been deployed, but the measurement requirements are changeable. It provides a simple and fast way to achieve high-sensitivity acoustic detection through DAS.

Abstract: Fiber distributed optical fiber acoustic sensor (DAS) is generally used in distributed long-distance acoustic/vibration measurement. We found that DAS with excellent performance of low self-noise and anti-fading in combination with the plastic structure in daily life as an acoustic transducer can achieve high-sensitivity acoustic measurement at a single point rather than designing a state-of-the-art acoustic transducer or using special enhanced scattering fiber. The simple acoustic transducer we proposed for DAS can reach the sensitivity level of -106.5dB re. 1rad/μPa at a sensing range of 5.1 km, which can meet many demands on the industrial site.

Keywords: optical fiber; distributed acoustic sensing; phase-sensitive OTDR (optical time domain reflectometry)

1. Introduction

Fiber distributed acoustic sensor (DAS) based on Rayleigh scattering employs low-cost, existing common single-mode fiber (SMF) to achieve quantitative acoustic measurement of long distance, high spatial resolution, and high sensitivity[1][2]. These advantages make DAS widely used in fields such as third-party interference (TPI) and leakage detection of pipelines[1][3], seismic [4][5], perimeter safety[6][7], traffic flow[8][9], etc.

Among DAS based on Rayleigh scattering, phase-sensitive OTDR optical time domain reflectometry (φOTDR), which can quantitatively measure the phase of Rayleigh scattering, has achieved commercial success because it not only has the common advantages of DAS but also is relatively low-cost[10][11]. However, due to the ultra-low Rayleigh scattering intensity, the acoustic sensitivity of φOTDR is hard to be improved[12]. For example, the sensitivity of the φOTDR used in seismic is still far lower than that of the traditional geophone[1]. Recently, more work turned to increase the distributed backscattering throughout the fiber, substantially improving the sensitivity and significantly suppressing the fading [2][13]. But it is still a great challenge for DAS to detect ultra-weak sounds like airborne sounds. The main reason is that the sound pressure coefficient of the optical fiber is minimal, which is too hard to quantify such a small phase change even using the state-of-the-art DAS[14]. The main idea to solve this problem is to design a sound pressure transducer with exquisite structure[15][13]. Although the effect of these transducers has been proved to be excellent, special customized mechanical designs are required[15]. When there is an urgent need for high-sensitivity acoustic measurement on the industrial site, there is no time to customize special transducers and order special enhanced scattering optical fiber (uncommon in daily life). Suppose we can transform ordinary objects in life into the acoustic transducer. In that case, we can quickly meet such urgent measurement needs, which could significantly improve the flexibility of the deployment of DAS.

Preprints (www.preprints.org) | NOT PEER-REVIEWED | Posted: 20 October 2022 doi:10.20944/preprints202210.0293.v1

In this work, we obtain a DAS with low-self noise and anti-fading performance through multi-frequency probe and polarization diversity receiver (PDR) to reduce the dependence on special optical fibers and a well-designed transducer, making the system more versatile. Then we connect the DAS to SMF and obtain an ultra-simple sound wave transducer with a good performance by manually winding the SMF to an ordinary plastic bottle. This way, we can quickly and flexibly switch the measurement methods on site and realize simultaneous distributed and point acoustic measurements.

2. Principle and experiment setup

The multi-frequency probes and PDR scheme has been proven effective in suppressing fading of φOTDR[12][16]. This paper adopts LFM-φOTDR with multi-frequency probe and PDR as the DAS, whose system structure is shown in Fig. 1.

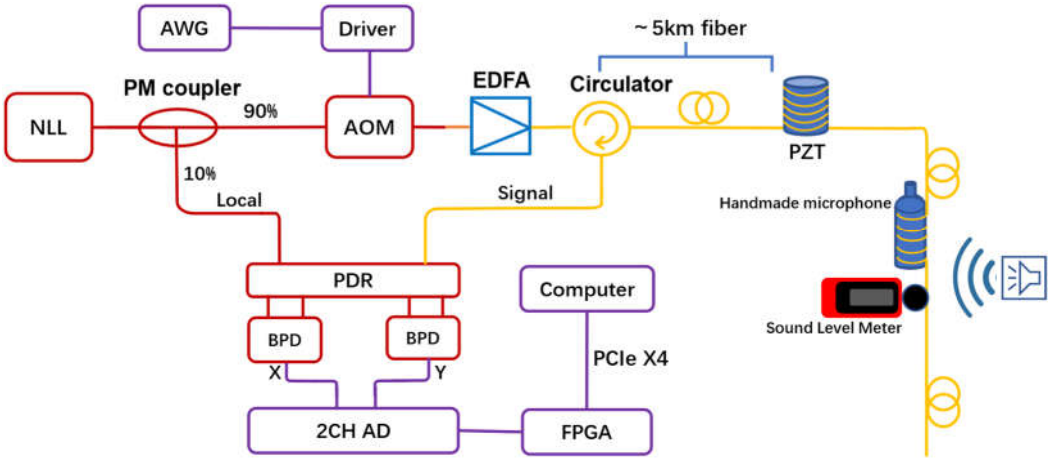

Figure 1. The DAS system based on multi-frequency and PDR receiver.

The light emitted by a narrow linewidth laser (NLL) with a low phase noise first passes through a polarization maintaining (PM) coupler. An acousto-optic modulator modulates 90% of the light to generate probe light. 10% of the light as a local oscillator signal can be expressed as:

$$E_L(t) = \sqrt{P_L}\exp(j\omega_c t) \tag{1}$$

P_L is the power of the local light. One wideband AWG generates LFM pulses, whose sweep range of two adjacent interrogation periods is 150M~200M (n=1) and 200M~250M (n=2), respectively,

$$s_n(t) = W\left(\frac{t}{T_p}\right)\exp j\left[2\pi f_{n,0}t + \pi\kappa t^2\right] \tag{2}$$

where $f_{n,0}$ represents the initial frequency of the nth LFM pulse, and κ Represents the chirp rate. LFM pulse of these two frequencies (pulse width T_p 2μs) is amplified by the power amplifier to drive the acoustic-optic modulator AOM to generate multi-frequency LFM pulse light. We use pulse EDFA to amplify the multi-frequency LFM pulse light to increase the power entering the optical fiber. Here, we need to avoid nonlinear effects, such as modulation instability [], caused by the system with excessive power injected into the fiber. The light field of the probe light entering the optical fiber can be expressed as:

$$E_{p,n}(t) = \sqrt{P_P}W\left(\frac{t}{T_p}\right)\exp j\left[\omega_c t + 2\pi f_{n,0}t + \pi\kappa t^2\right] \tag{3}$$

When the probe light is injected into the fiber to be tested, Rayleigh scattered light returns to the receiver through port two and port three of the circulator in turn. The returned Rayleigh backscattered light field can be expressed as

Preprints (www.preprints.org) | NOT PEER-REVIEWED | Posted: 20 October 2022 doi:10.20944/preprints202210.0293.v1

$$E_{R,n}(t) = \sum_{i=1}^{N} E_i W\left(\frac{t-\tau_i}{T_p}\right) \exp j\left[\omega_c(t-\tau_i) + 2\pi f_{n,0}(t-\tau_i) + \pi\kappa(t-\tau_i)^2\right] \quad (4)$$

where N is the total number of scattering points in the fiber, E_i is the electric field intensity of the scattered light at each scattering point, τ_i is the time delay of Rayleigh backscattered light generated at a certain position i on the optical fiber returning to the receiver. PDR is used to reduce polarization fading. The local oscillator and Rayleigh scattered light are mixed in the PDR, and then the Rayleigh scattered light of two polarization states is detected by two balanced detectors with a bandwidth of 350M, where the detected x-polarization signal can be expressed as

$$\begin{aligned} i_{n,x}(t) &\propto \Im\{E_{Rn}(t) \cdot E_L^*(t)\} \\ &= \sum_{i=1}^{N} A_i W\left(\frac{t-\tau_i}{T_p}\right) \sin\{2\pi f_{n,0}(t-\tau_i) + \pi\kappa(t-\tau_i)^2 - \omega_c\tau_i\} \end{aligned} \quad (5)$$

where * is the complex conjugate sign, and A is the amplitude of Rayleigh backscattered light converted into electrical signal by BPD. Then $i(t)$ is converted to digital signal by two 250M A/D converters and demodulated in real-time by high-speed FPGA. We use Hilbert transform to change the real signal $i(t)$ into the complex signal, which can be expressed as follows in the x polarization:

$$\begin{aligned} i_{n,x}(t) &= \int_0^{\mathrm{T}} A(\tau) W\left(\frac{t-\tau}{T_p}\right) \exp\{j\left[2\pi f_{n,0}(t-\tau) + \pi\kappa(t-\tau)^2 - \omega_c\tau\right]\} d\tau \\ &= h(t) \otimes s_n(t) \end{aligned} \quad (6)$$

where T is the total round-trip time in the optical fiber, $h(t)$ is defined as the impact response of the fiber under test (FUT). We generate the Matching filter $s_n^*(-\mathrm{t})$ on FPGA, and convoluted with $i_{n,x}(t)$ to obtain Rayleigh scattering signal in x polarization direction after pulse compression

$$I_{n,x}(t) = h(t) \otimes s_n(t) \otimes s_n^*(-\mathrm{t}) \quad (7)$$

At last, we get four complex vectors $I_{1,x}(t)$, $I_{1,y}(t)$, $I_{2,x}(t)$, $I_{2,y}(t)$. The relative relationship of these four complex vectors in time is shown in Fig. 2.

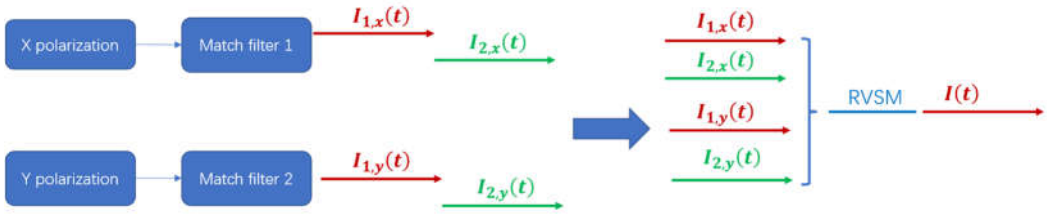

Figure 2. The space and time relationship of $I_{1,x}(t)$, $I_{1,y}(t)$, $I_{2,x}(t)$, $I_{2,y}(t)$.

$\boldsymbol{I_{2,x}(t)}$ $\boldsymbol{I_{2,y}(t)}$ **is 0.**04ms later than $I_{1,x}(t)$, $I_{1,y}(t)$, we first delay the $I_{1,x}(t)$, $I_{1,y}(t)$ by 0.04 ms, and then use the rotated vector sum method (RVSM) to synthesize the four complex vectors. Since the randomness of Rayleigh scattering intensity is related to the polarization and frequency of the detection light, the four signals can play a significant anti-fading effect by RVSM. Therefore, within 0.08ms, one complex vector signal is obtained by RVSM, so the interrogation frequency of the system is 12.5kHz, which can respond to acoustic signals with a frequency less than 6.25kHz, covering ordinary acoustic frequencies such as mechanical vibration and voice. The complex vector signal is transmitted to the upper computer through the PCIe x4 bus for spatial difference and unwinding operations. Finally, the acoustic signal of the entire optical fiber is demodulated in real-time.

3. Results

3.1. Anti-fading effect of the DAS

The route of the FUT is: 5.1km bare SMF reel - 20m SMF wound on PZT - 100m jumper - self-made microphone with 20m fiber – 0.8km bare optical fiber reel. We applied

Preprints (www.preprints.org) | NOT PEER-REVIEWED | Posted: 20 October 2022 doi:10.20944/preprints202210.0293.v1

a signal with a frequency of 400 Hz to the PZT and recorded the 480 meters signal around the PZT when using the different number of polarization and frequency, as shown in Fig. 3, We can see that the four signals of the time-differential phase of "1-polarization-1-frequency" have many fading points(Fig. 3 (a)(b)(c)(d)), and phase(Fig. 3(f)) and its time differential phase (Fig. 3(e)) synthesized by "2-polarization-2-frequency" almost have no fading point, which means that the system can recover and output high-quality acoustic signals consistently.

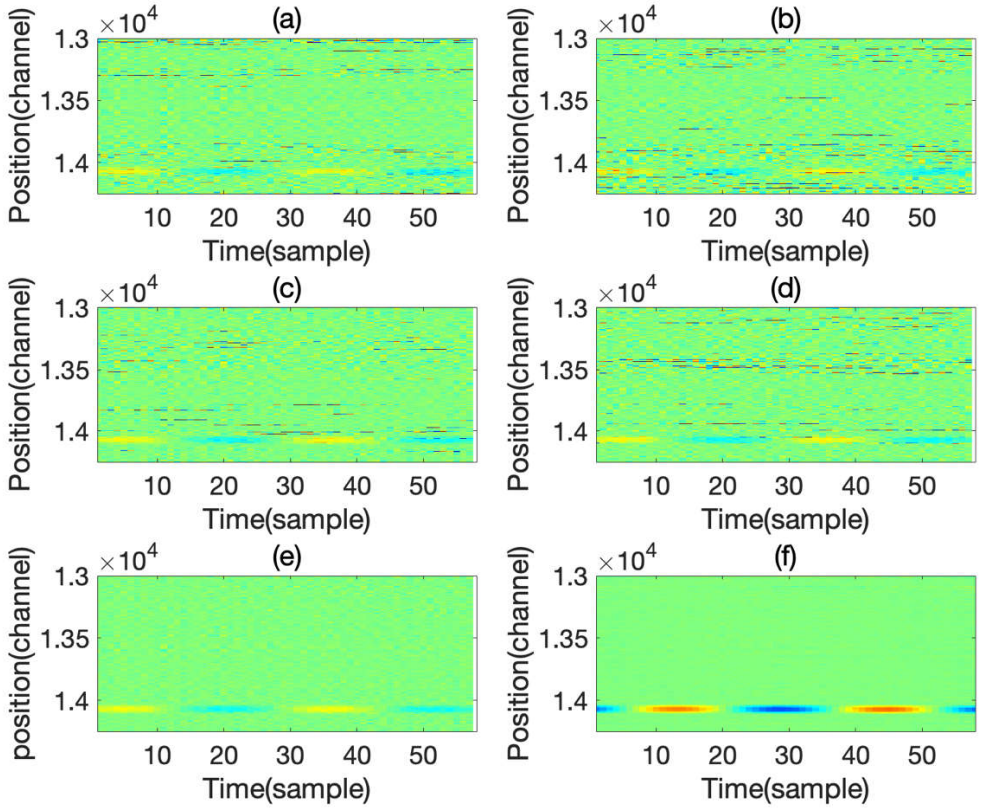

Figure 3. The time differential phase waterfall demodulated by (a)1st frequency of X polarization; (b)2nd frequency of X polarization; (c)1st frequency of Y polarization; (d)2nd frequency of Y polarization; the time differential phase (e) and phase (f) waterfall synthesized by a "2-polarization-2-frequency".

3.2. Fabricate of microphone

When we talk close to the plastic bottle, if we hold the plastic bottle, we will feel noticeable vibration, which inspires us if the fiber is wound onto the plastic bottle, the phase change of Rayleigh scattering will be much larger due to the increase of strained fiber length. When the system has good anti-fading performance, we chose an ordinary empty plastic drink bottle with a diameter of ~6.5 cm and a total length of ~23 cm was used as the acoustic transducer structure. We wound the 20m fiber in the regular and shallow groove on the bottle. The fiber was wound slightly tight to obtain an initial strain. Finally, we use high-temperature tape to fix the fiber on the bottle. The handmade microphone is shown in Fig. 4. We put a Sound level meter (SLM) together with the microphone to measure the sound level of the speaker. To match the fiber length on the microphone, the gauge length of DAS in this experiment is set to 22.4m, a little longer than the length of the fiber wound onto the microphone (20m).

Preprints (www.preprints.org) | NOT PEER-REVIEWED | Posted: 20 October 2022 doi:10.20944/preprints202210.0293.v1

Figure 4. Handmade microphone (up) and Sound level meter SLM (down).

3.3. The performance of DAS and handmade microphone

To test the performance of this handmade microphone, we placed a speaker at 50cm from the microphone and then let the speaker generate sound waves with a frequency of 500Hz and a decibel of 84dB (tested by the SLM near the microphone). At the same time, we applied a 200Hz 3V drive signal to the PZT. The waterfall signals of 6km fiber collected by the DAS system are shown in Fig. 5.

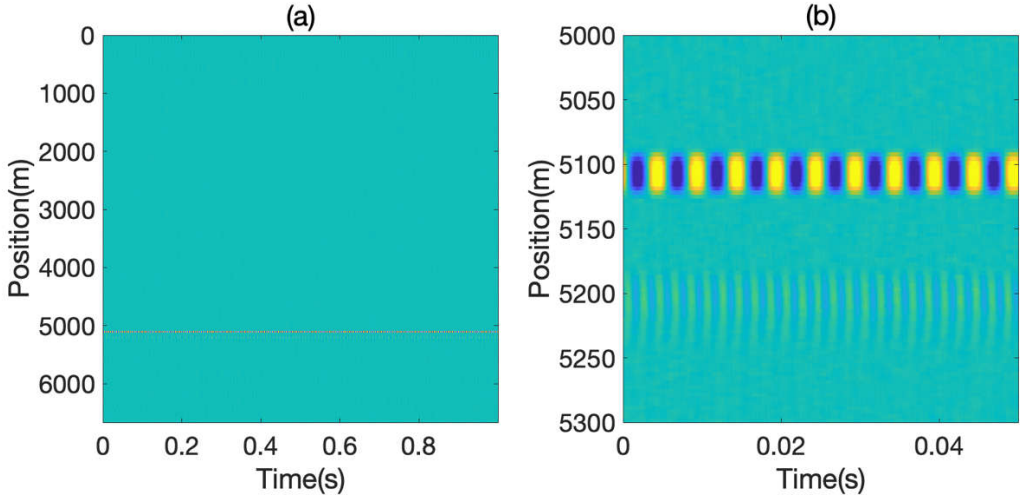

Figure 5. The phase waterfall of (a)6km fiber and (b)near PZT and microphone.

We indexed the phase at the PZT and handmade microphone positions, respectively, as shown in Fig. 5(a)(b). It should be noted that since the PZT and the microphone are not placed in a vibration isolation room, there will be some environmental interference, especially the low-frequency sound mixed in the acquired signal. We can roughly estimate that the background noise of the system (from Fig. 6(c) (d)) is $-60dB\ rad^2/Hz$, a minimum detectable strain of ~10 pε/√Hz. The phase change generated by the handmade microphone was ~1.5 rad. Considering the SPL of 84 dB, the measured sensitivity is -106.5 dB re.1rad/μPa.

Preprints (www.preprints.org) | NOT PEER-REVIEWED | Posted: 20 October 2022 doi:10.20944/preprints202210.0293.v1

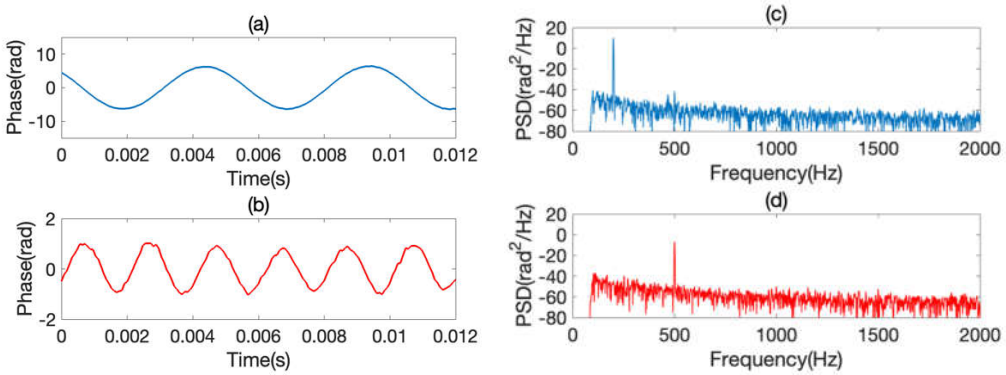

Figure 6. phase at the positions of (a)PZT and (b)handmade microphone. PSD of phase at the positions of (c)PZT and (d)handmade microphone.

Then we test the microphone's normalized frequency response by tuning the speaker's frequency from 200Hz to 1000Hz in step of 50Hz (at a fixed volume), as shown in Fig. 7. The largest response frequency is around ~450Hz, which may be related to the fact that the material of the microphone is plastic, whose elastic modulus is relatively large. Therefore, the handmade microphone is more suitable for detecting low-frequency mechanical vibration. If the frequency band of the detected sound is higher, the material with a small elastic modulus should be selected.

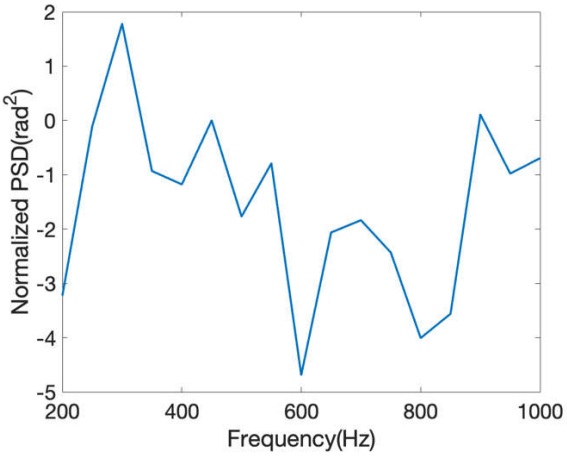

Figure 7. Normalization frequency response of the handmade microphone.

3.4. The simulation sound of valve acquisition by the handmade microphone

To simulate the ability of the handmade microphone to deploy in the industrial field, we played two mechanical audio files of an open dataset [17] for malfunctioning industrial machine investigation and inspection (MIMII dataset). The sound file we played was generated by valves. The first part of the sound file we played was generated by the normal valves and the second part was abnormal. The signal recorded by our microphone is processed by a high pass filter (the stop edge frequency is 80Hz, the pass edge frequency is 100Hz) to remove most of the DC noise generated by temperature or low-frequency vibration. The recorded signal of the valve can be seen in Fig. 8 and downloaded in Supplement 1. The rhythmic working sound of the valve and the background noise can be clearly heard.

Preprints (www.preprints.org) | NOT PEER-REVIEWED | Posted: 20 October 2022 doi:10.20944/preprints202210.0293.v1

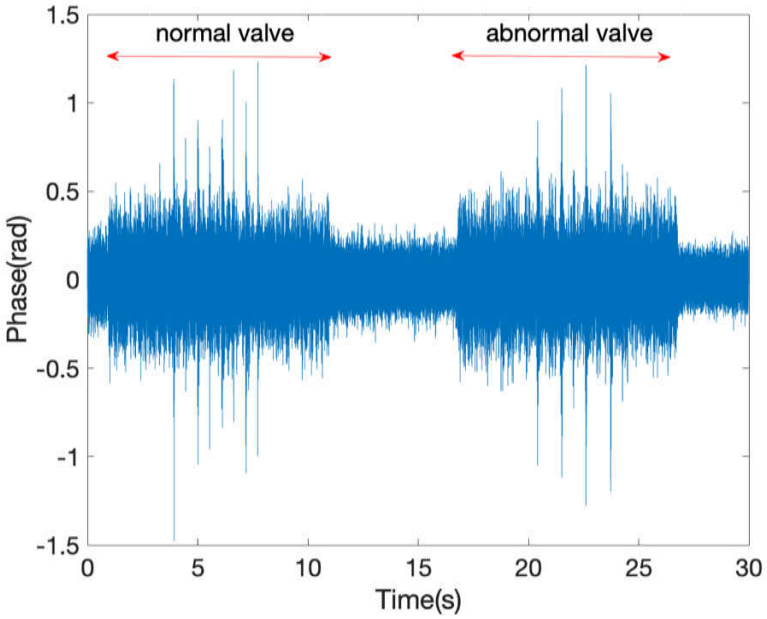

Figure 8. The recovered simulated valve sound by the handmade microphone.

4. Discussion and Conclusions

This paper presents a DAS with a hybrid distributed/point topology: most fiber is straight to complete distributed measurement, but at the same time, to improve the sensitivity of some points, fibers can be wound onto transducers that can improve acoustic wave reception. We have proved through experiments that transducers are not must over-meticulously designed and machined if the performance of DAS is good enough and the conditions are limited. We can wind fiber onto common objects (such as plastic bottles) around us, and then we can achieve high-sensitive acoustic measurements quickly. The fabrication of this microphone is simple: it only takes 20 minutes to wind a 20-meter-long optical fiber onto a drink plastic bottle.

In the industrial field, the measurement requirements may be urgent, so it is necessary to realize this flexible topology simply. For example, since the vibration wave generated by the TPI has a large scope of action, the fiber parallel to the power cable is used to detect TPI events distributedly. Because the power cable accessories are more prone to insulation failure, we can install simple microphones at the cable accessories, which can significantly improve the acoustic sensitivity at this position so that it has better partial discharge detection capability. We believe that the simultaneous distributed and point acoustic measurement in a handy and cost-efficient way will benefit the DAS application in industries.

Author Contributions: Conceptualization, J. T. and F.P..; methodology, J. T.; software, F.P.; validation, M.H; formal analysis, M.H; investigation, F.P.; resources, J. T.; data curation, X.Z and F.P.; writing—original draft preparation, J. T.; writing—review and editing, F.P.; visualization, M.H. All authors have read and agreed to the published version of the manuscript.

Funding: This work was partially supported by the National Natural Science Foundation of China under Grant 51907135, partly by the Fundamental Research Funds for the Central Universities under Grant YJ201654, and partly by Sichuan Science and Technology Program under Grant 2020YFG0029.

Data Availability Statement: The data presented in this study are available upon request from the corresponding author.

Conflicts of Interest: The authors declare no conflict of interest.

References

1. Ashry, I.; Mao, Y.; Wang, B.; Hveding, F.; Bukhamsin, A.; Ng, T.K.; Ooi, B.S. A Review of Distributed Fiber–Optic Sensing in the Oil and Gas Industry. *J. Lightwave Technol.* **2022**, *40*, 1407–1431, doi:10.1109/JLT.2021.3135653.
2. Sun, Y.; Li, H.; Fan, C.; Yan, B.; Chen, J.; Yan, Z.; Sun, Q. Review of a Specialty Fiber for Distributed Acoustic Sensing Technology. *Photonics* **2022**, *9*, 277, doi:10.3390/photonics9050277.
3. Muggleton, J.M.; Hunt, R.; Rustighi, E.; Lees, G.; Pearce, A. Gas Pipeline Leak Noise Measurements Using Optical Fibre Distributed Acoustic Sensing. *Journal of Natural Gas Science and Engineering* **2020**, *78*, 103293, doi:10.1016/j.jngse.2020.103293.
4. Martuganova, E.; Stiller, M.; Norden, B.; Henninges, J.; Krawczyk, C.M. 3D Deep Geothermal Reservoir Imaging with Wireline Distributed Acoustic Sensing in Two Boreholes. *Solid Earth* **2022**, *13*, 1291–1307, doi:10.5194/se-13-1291-2022.
5. Williams, E.F.; Fernández-Ruiz, M.R.; Magalhaes, R.; Vanthillo, R.; Zhan, Z.; González-Herráez, M.; Martins, H.F. Distributed Sensing of Microseisms and Teleseisms with Submarine Dark Fibers. *Nat Commun* **2019**, *10*, 5778, doi:10.1038/s41467-019-13262-7.
6. Zhu, P.; Xu, C.; Ye, W.; Bao, M. Self-Learning Filtering Method Based on Classification Error in Distributed Fiber Optic System. *IEEE Sensors J.* **2019**, *19*, 8929–8933, doi:10.1109/JSEN.2019.2907117.
7. Li, Z.; Zhang, J.; Wang, M.; Zhong, Y.; Peng, F. Fiber Distributed Acoustic Sensing Using Convolutional Long Short-Term Memory Network: A Field Test on High-Speed Railway Intrusion Detection. *Opt. Express* **2020**, *28*, 2925, doi:10.1364/OE.28.002925.
8. Xu, S.; Qin, Z.; Zhang, W.; Xiong, X. Monitoring Vehicles on Highway by Dual-Channel φ-OTDR. *Applied Sciences* **2020**, *10*, 1839, doi:10.3390/app10051839.
9. Chambers, K. Using DAS to Investigate Traffic Patterns at Brady Hot Springs, Nevada, USA. *The Leading Edge* **2020**, *39*, 819–827, doi:10.1190/tle39110819.1.
10. Wang, Y.; Zheng, H.; Lu, C. High-Sensitivity Distributed Relative Salinity Sensor Based on Frequency-Scanning φ-OTDR. *Opt. Express* **2022**, *30*, 22860, doi:10.1364/OE.458200.
11. Wang, Z.; Lu, B.; Ye, Q.; Cai, H. Recent Progress in Distributed Fiber Acoustic Sensing with Φ-OTDR. *Sensors* **2020**, *20*, 6594, doi:10.3390/s20226594.
12. Ogden, H.M.; Murray, M.J.; Murray, J.B.; Kirkendall, C.; Redding, B. Frequency Multiplexed Coherent Φ-OTDR. *Scientific Reports* **2021**, 13.
13. Li, H.; Sun, Q.; Liu, T.; Fan, C.; He, T.; Yan, Z.; Liu, D.; Shum, P.P. Ultra-High Sensitive Quasi-Distributed Acoustic Sensor Based on Coherent OTDR and Cylindrical Transducer. *J. Lightwave Technol.* **2020**, *38*, 929–938, doi:10.1109/JLT.2019.2951624.
14. Hocker, G.B. Fiber-Optic Sensing of Pressure and Temperature. *Appl. Opt., AO* **1979**, *18*, 1445–1448, doi:10.1364/AO.18.001445.
15. Wu, Y.; Gan, J.; Li, Q.; Zhang, Z.; Heng, X.; Yang, Z. Distributed Fiber Voice Sensor Based on Phase-Sensitive Optical Time-Domain Reflectometry. *IEEE Photonics J.* **2015**, *7*, 1–10, doi:10.1109/JPHOT.2015.2499539.
16. Zhang, J.; Wu, H.; Zheng, H.; Huang, J.; Yin, G.; Zhu, T.; Qiu, F.; Huang, X.; Qu, D.; Bai, Y. 80 Km Fading Free Phase-Sensitive Reflectometry Based on Multi-Carrier NLFM Pulse Without Distributed Amplification. *J. Lightwave Technol.* **2019**, *37*, 4748–4754, doi:10.1109/JLT.2019.2919671.
17. Purohit, H.; Tanabe, R.; Ichige, K.; Endo, T.; Nikaido, Y.; Suefusa, K.; Kawaguchi, Y. MIMII Dataset: Sound Dataset for Malfunctioning Industrial Machine Investigation and Inspection 2019.